Ocean Dynamics (2017) 67:799–811
DOI 10.1007/s10236-017-1047-2

Erosion characteristics and horizontal variability for small erosion depths in the Sacramento-San Joaquin River Delta, California, USA

David H. Schoellhamer[1,2] · **Andrew J. Manning**[3,4,5] · **Paul A. Work**[1]

Received: 29 January 2016 / Accepted: 8 March 2017 / Published online: 24 April 2017

Abstract Erodibility of cohesive sediment in the Sacramento-San Joaquin River Delta (Delta) was investigated with an erosion microcosm. Erosion depths in the Delta and in the microcosm were estimated to be about one floc diameter over a range of shear stresses and times comparable to half of a typical tidal cycle. Using the conventional assumption of horizontally homogeneous bed sediment, data from 27 of 34 microcosm experiments indicate that the erosion rate coefficient increased as eroded mass increased, contrary to theory. We believe that small erosion depths, erosion rate coefficient deviation from theory, and visual observation of horizontally varying biota and texture at the sediment surface indicate that erosion cannot solely be a function of depth but must also vary horizontally. We test this hypothesis by developing a simple numerical model that includes horizontal heterogeneity, use it to develop an artificial time series of suspended-sediment concentration (SSC) in an erosion microcosm, then analyze that time series assuming horizontal homogeneity. A shear vane was used to estimate that the horizontal standard deviation of critical shear stress was about 30% of the mean value at a site in the Delta. The numerical model of the erosion microcosm included a normal distribution of initial critical shear stress, a linear increase in critical shear stress with eroded mass, an exponential decrease of erosion rate coefficient with eroded mass, and a stepped increase in applied shear stress. The maximum SSC for each step increased gradually, thus confounding identification of a single well-defined critical shear stress as encountered with the empirical data. Analysis of the artificial SSC time series with the assumption of a homogeneous bed reproduced the original profile of critical shear stress, but the erosion rate coefficient increased with eroded mass, similar to the empirical data. Thus, the numerical experiment confirms the small-depth erosion hypothesis. A linear model of critical shear stress and eroded mass is proposed to simulate small-depth erosion, assuming that the applied and critical shear stresses quickly reach equilibrium.

Keywords Erosion · Cohesive sediment · Sacramento-San Joaquin River Delta · Erosion microcosm · Critical shear stress · Estuary · Estuarine · Sediment bed

This article is part of the Topical Collection on the *13th International Conference on Cohesive Sediment Transport in Leuven, Belgium 7–11 September 2015*

Responsible Editor: Joris Vanlede

✉ David H. Schoellhamer
dschoell@usgs.gov

Andrew J. Manning
A.Manning@hrwallingford.com; A.Manning@hull.ac.uk

[1] US Geological Survey, California Water Science Center, 6000 J Street, Placer Hall, Sacramento, CA 95819, USA

[2] US Geological Survey, 2130 SW 5th Avenue, Portland, OR 97201, USA

[3] HR Wallingford, Howbery Park, Wallingford, Oxfordshire OX10 8BA, UK

[4] Geography & Geology, School of Environmental Sciences, Faculty of Science & Engineering, University of Hull, Hull HU6 7RX, UK

[5] University of Plymouth, Plymouth, Devon PL4 8AA, UK

1 Introduction

Erosion of cohesive sediment is commonly conceptualized and simulated as a depth-dependent process (Hayter 1986; Grabowski et al. 2011). As sediment is eroded, the critical shear stress τ_c of the remaining sediment increases, the excess shear stress is reduced, and the rate of erosion decreases. Consolidation and compaction are the primary bed processes

responsible for the depth dependence. Depth-dependent erosion models invoke the assumption that the erosive properties of the bed are uniform (i.e., homogeneous) over the horizontal area of a computational grid cell, typically on the order of meters. Variability at the subgrid scale is not considered.

In situations with shallow water depths and small increases in suspended-sediment concentration (SSC) during a tidal cycle, the erosion depth can be as small as a few floc diameters. For example, in the Sacramento-San Joaquin River Delta (Delta), California, USA, typical water depth is 5 m, bed bulk density is 600 kg/m^3, and SSC may increase 10 mg/l from slack to maximum tide. Assuming that the SSC increase is due to erosion and that erosion is uniformly distributed horizontally, the depth of erosion would be 80 μm, about the diameter of one floc (Ganju et al. 2007; Manning and Schoellhamer 2013). We define small-depth erosion as erosion depths equal to order one floc diameter assuming that erosion is uniformly distributed.

Some studies consider the variation of the sediment surface and erosive properties at small horizontal scales. Grabowski et al. (2011) reviewed several field studies that found significant horizontal variations on the centimeter to meter scale. In addition, Bentley et al. (2014) collected x-radiographs of a tracer placed on a mudflat and found biogenic structures at millimeter to centimeter scale at the sediment surface. Van Prooijen and Winterwerp (2010) consider erosion due to stochastic turbulent shear stress distribution and horizontally heterogeneous erosion parameters.

In this study, we test the hypothesis that small-depth erosion is controlled by horizontal heterogeneity of erosive properties in addition to depth dependence. The scale of the heterogeneity is on the orders of millimeters and centimeters and would typically not be resolved by a horizontal modeling grid. Inclusion of this variability requires a stochastic approach (van Prooijen and Winterwerp 2010). Temporal and spatial variability of applied shear stress is not considered. An erosion microcosm was used to determine erosive characteristics of cores collected from the Delta. Small-depth erosion was observed, and the surface of the cores generally appeared to be heterogeneous. A shear vane was used to obtain a quantitative estimate of horizontal heterogeneity for use in a numerical model. A numerical model of microcosm erosion for a core with horizontally heterogeneous erosion properties was developed to compare the characteristics of horizontally heterogeneous and homogeneous erosion. The results were analyzed assuming horizontally homogeneous erosive properties and compared to the prescribed initial condition. An approach for simulating small-depth erosion is proposed, invoking the assumption that an increase in applied bed shear stress results in rapid erosion and increase of the critical shear stress of the bed, and re-equilibration. This assumption removes the need for an empirically derived erosion coefficient.

2 Field methods

We determined physical and erosive properties of cohesive sediment in the Sacramento-San Joaquin River Delta (Fig. 1). The Delta is composed of interconnected tidal channels that surround subsided and leveed islands. Much of our data was collected from a site used by Jones et al. (2008) to study wind waves in Franks Tract, a former subsided island which became permanently flooded after a levee break. The primary source of freshwater is the Sacramento River that enters the Delta from the north (Wright and Morgan 2015). At its western boundary, the Delta is connected to San Francisco Bay and ultimately the Pacific Ocean. Freshwater diversions from the Delta require that saltwater be kept out of the Delta through managing water releases from upstream reservoirs. The Mediterranean climate features rainfall and runoff during the winter wet season and little rainfall or natural runoff during the dry summer season. Suspended sediment is the primary cause of turbidity (Ganju et al. 2007), and reduced turbidity and suspended sediment (Hestir et al. 2013) have been coincident with declines of native fish populations that favor turbid water (Nobriga et al. 2005). Tidal marsh sustainability depends on adequate supply of suspended sediment (Swanson et al. 2015).

2.1 Erosive properties

Sediment cores were collected and eroded in an erosion microcosm, and the data were analyzed with an erosion model. The basic procedure for this study is similar to that described by Dickhudt et al. (2011):

1. Collect sediment cores: Two sediment cores are collected from a study site with a gravity GOMEX corer (the use of firm, trade, and brand names in this report is for identification purposes only and does not constitute endorsement by the US Geological Survey) lowered to the bed from a small boat. The cores are typically 10–30 cm deep, and water is retained above the sediment in the corer. After raising the corer back onto the boat, a 10-cm-diameter tube is immediately pushed into the top of each core to collect a sample. Samples are disturbed as little as possible, and the erosion experiment was conducted on shore within an hour. Andersen et al. (2010) found that erosion of cores from an intertidal mudflat carefully returned to the laboratory was similar to erosion measured in situ. In addition, ambient water was collected to pump into the erosion microcosm.
2. Erode the cores: A piston inserted into the bottom of the tube is used to push the sediment surface up to 10 cm from the top of the tube. The core is eroded using a dual core University of Maryland Center for Environmental Science—Gust Erosion Microcosm System. Two cores are eroded simultaneously. A disk rotates at the water surface at the top of the tube, and water is pumped radially from the outside toward

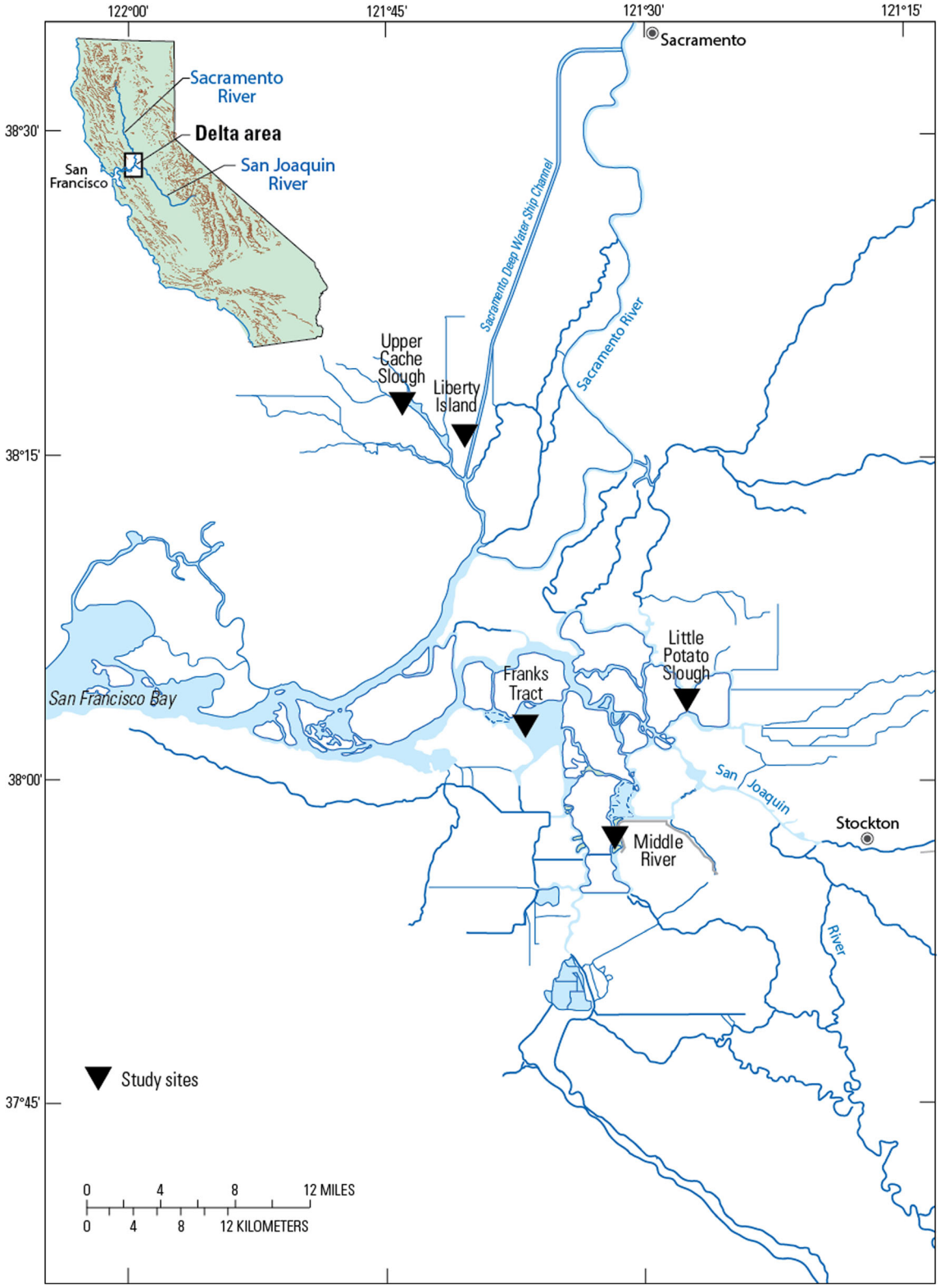

Fig. 1 Sacramento-San Joaquin River Delta study area

the center of the tube at predetermined rates that provide nearly uniform and known shear stresses at the sediment/water interface (Gust and Mueller 1997). Turbidimeters continuously monitor the effluent. A 0.01-Pa shear stress τ is initially applied to flush and stabilize the system, and τ is subsequently increased stepwise over a period of about 3 h (Table 1). Water samples are collected during each step to calibrate turbidity to SSC.

3. Analyze the SSC time series data: The time series of erosion rate (kg/m^2/s) is calculated by applying the principle of conservation of mass to the water volume of the erosion microcosm, and the erosion model of Sanford and Maa (2001) is used to calculate erosion parameters. The erosion rate E for an experiment as a function of mass eroded (m) and time (t) is

$$E(m,t) = M(m)\,[\tau(t) - \tau_c(m)] \tag{1}$$

Critical shear stress τ_c is calculated at the end of each step and is assumed to increase with m which in turn increases with erosion depth. The erosion rate coefficient $M(m)$ is assumed to be a constant for each step.

A total of 34 cores from five sites in the Delta were analyzed from November 2011 to November 2014. Fifteen cores were collected from Franks Tract, 10 from upper Cache Slough, 6 from Little Potato Slough, 2 from Middle River, and one from Liberty Island (Fig. 1). Subsamples of the top 1 cm of most cores were collected to determine particle size distribution, with a Coulter counter, and water content w. Size is represented as the mass fraction of (fine) sediment less than 63 μm in diameter. Comparisons of dependent and independent variables use Spearman's rho and Kendall's tau nonparametric tests to determine the presence of a monotonic trend (Helsel and Hirsch 1992). During an experiment, the initial critical shear stress is usually less than 0.4 Pa and the critical shear stress increases above 0.4 Pa. Thus, the total mass eroded during an experiment when the critical shear stress reaches 0.4 Pa ($m_{0.4}$) is a convenient quantity for expressing the quantity of eroded sediment from a core (Dickhudt et al. 2011). We also calculate the solid volume fraction of mud matrix

$$\varphi_{sm} = \frac{1 - f_s}{\frac{1}{\varphi_{stot}} - f_s} \tag{2}$$

where f_s is the mass fraction of sand and φ_{stot} is bed solid volume fraction equal to one minus the porosity

$$p = \frac{V_w}{V_w + V_s} = \frac{x/\rho_w}{\frac{x}{\rho_w} + 1/\rho_s} \tag{3}$$

where V_w is the volume of water, V_s is the volume of sediment, ρ_w is the density of water equal to 1000 kg/cm^3, ρ_s is the density of solids assumed to equal 2650 kg/cm^3, and

$$x = \frac{w}{1 - w} \tag{4}$$

2.2 Horizontal heterogeneity of shear strength

We used a handheld shear vane to estimate the spatial heterogeneity of the surface strength of five cores collected at Franks Tract in the Delta on July 30, 2014. A vane with four fins 33 mm in diameter and 49.5 mm tall was inserted into the sediment until the top of the vane was at the sediment surface. The vane is supposed to be inserted further such that the top of the sheared sediment is confined, so our readings are not true shear strength. We did not insert further, because our interest was in the variability of strength near the surface rather than a standard measure of shear strength. We assume that the estimated heterogeneity of the top 49.5 mm of the core represents the heterogeneity of the surface. Care was taken to insert the vane straight with little side-to-side movement. Then, the dial was slowly spun; the reading increases as the spring was loaded, until the soil failed when the spring was no longer loading; and the vane started rotating. The dial reading at failure in N-m was recorded, and the dial resets to zero for the next reading. The vane dial had two scales on it—one intended for a 19-mm-diameter vane and another for a 33-mm-diameter vane. Failure occurred soon after the test started, and the scale intended for the 19-mm vane had better resolution where failure occurred than the 33-mm vane scale; thus, we used the 19-mm vane scale. The dial reading is proportional to the shear strength.

Table 1 Applied shear stresses and flow rates for water temperature of 15 °C

Applied shear stress τ_b in Pa	Flow rate Q in ml/min
0.01	27.1
0.05	82.3
0.10	118
0.15	142
0.20	160
0.30	186
0.45	210
0.60	223

We took surface readings in each corner and midpoint for a total of eight readings per core. One deep reading (bottom of vane 152.4 mm below the surface) was taken at the center of each core, which is within the suggested depth for measurement to properly obtain a measure of shear strength. In a couple of cases, water broke out from the core and the location of vane measurements was slightly shifted to avoid being too close to a scour tunnel in the corer. If water was retained, it was removed by bailing and a pump. After each core was collected, a 1–2 m of line was let out on the boat anchor so we would have fresh sediment for the next core. The surface was mostly covered with tubes built by a freshwater worm *Manayunkia speciosa* and some macroalgae (Fig. 2). A total of five cores were collected and measured for a total

Fig. 2 Sediment surface of a core from Franks Tract, July 30, 2014. The surface was mostly covered with tubes built by a freshwater worm *Manayunkia speciosa* and some macroalgae. The core is in the 10-cm-diameter erosion microcosm, and the 1.91-cm-diameter gray plastic disk in the center is to prevent erosion where shear stress is known to be greater than elsewhere during the experiment

of 39 readings. The first core had a midpoint that we did not sample correctly, so it was not included.

3 Results

3.1 Erosive properties

For the 34 cores, water depth above the core when collected, fine fraction, and water content all co-varied. As water depth increased, increases of the fine fraction and water content were statistically significant (Table 2). Greater shear stress in shallower water where wind waves are prevalent, thus winnowing fine sediments, is a likely explanation. As the fine fraction increased, there was a statistically significant increase in water content.

Erosion occurred as type I depth-limited erosion (Sanford and Maa 2001). A step increase in applied shear stress (Table 1) produced a temporary increase in SSC that was returning to ambient values by the end of the typically 20-min (1200 s) long step (Fig. 3). Critical shear stress increased as mass was eroded, and the applied shear stress was increased. The mass eroded when critical shear stress was 0.4 Pa increased with water depth, fine fraction, and water content (Table 2). Initial critical shear stress generally did not covary with water depth, fine fraction, or water content. Erosion parameters showed no seasonal signal, possibly due to drought during the study, insufficient temporal resolution, or insufficient study duration. Erosion rate coefficient $M(m)$ generally increased with eroded mass for 27 of 34 cores.

Of the 34 cores tested, 15 were collected from Franks Tract (Fig. 1) so these data provide the largest data set that excludes any confounding intersite variations. Franks Tract is a shallow open water body that is subject to wind waves (Jones et al. 2008) and likely sediment resuspension; the mean water depth at coring sites was 2.6 m. Critical shear stress $\tau_c(m)$ and erosion rate coefficient $M(m)$ varied between cores (Figs. 4 and 5). Ten cores were collected from upper Cache Slough which is a channel. The mean water depth at coring sites was 5.2 m, and during predominant low freshwater flows, landward sediment transport in the Slough traps sediment (Morgan-King and Schoellhamer 2013). Thus, fine fraction, water content, and $m_{0.4}$ were greater in upper Cache Slough than in Franks Tract (Table 3). The appearance of $\tau_c(m)$ and $M(m)$ in upper Cache Slough is similar to Franks Tract, and thus, they are not shown.

Dickhudt et al. (2011) found that initial critical shear stress $\tau_c(0)$ increased as the solid volume fraction of mud matrix φ_{sm} increased for the York River and several other estuaries (Fig. 6). For this study, values of $\tau_c(0)$ less than about 0.15 Pa fall within the data from other estuaries but greater values of $\tau_c(0)$ are above the envelope of data from other estuaries.

3.2 Horizontal heterogeneity of shear strength

Shear vane readings were usually higher for the midpoint of the core than the corners (Figs. 7 and 8). The 75th percentile of the corner readings (5 N-m) was equal to the 25th percentile of the midpoint readings. The corners were closer to where the corer's jaws closed, and they had two perpendicular plates inserted nearby, not one plate, which perhaps disturbed and weakened the soil. To quantify horizontal shear stress heterogeneity, we separate these two populations.

Standard deviations are 35 and 26% of the mean for corner and midpoint readings, respectively. Thus, an approximation

Table 2 Significance (p value) of Spearman rho/Kendall tau tests for a monotonic trend

	Fine fraction	Water content	Initial τ_c	$m_{0.4}$
Water depth	*<0.002/0.000*	*0.006/0.007*	0.960/*0.004*	0.071/*0.003*
Fine fraction	–	*<0.002/0.000*	>0.2/0.285	*<0.002/0.000*
Water content	–	–	>0.2/0.359	*<0.002/0.003*
Initial τ_c	–	–	–	0.799/0.080

Statistically significant values with $p < 0.05$ are shown in italic. $m_{0.4}$ is the total mass eroded when the critical shear stress reaches 0.4 Pa

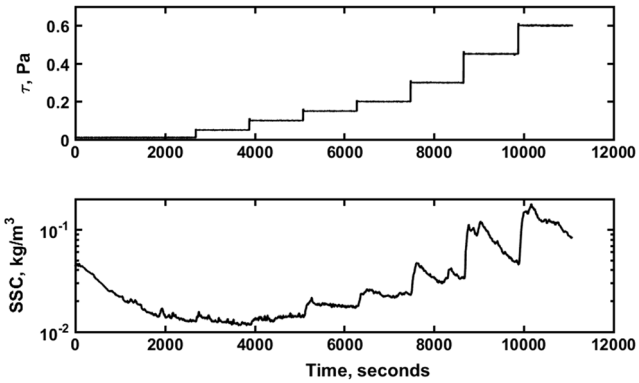

Fig. 3 Applied shear stress $\tau(t)$ and measured suspended-sediment concentration for a typical erosion experiment, Franks Tract, May 22, 2014, core 2

is that the standard deviation of the critical shear stress is 30% of the mean.

4 Hypothesis that erosion of small depths depends on horizontal heterogeneity

We hypothesize that small-depth erosion is controlled by horizontal heterogeneity in addition to depth dependence. The cores collected in this study often had benthic structures on the millimeter to centimeter scale which present a surface that is not horizontally uniform (Fig. 2). The Sanford and Maa (2001) erosion model used to analyze data from the erosion microcosm, however, assumes that the erosion parameters are horizontally homogeneous. Thus, for a uniformly applied shear stress, the erosion depth of the model is uniform. An alternative conceptual model is presented by van Prooijen and Winterwerp (2010) who consider erosion due to stochastic turbulent shear stress distribution and horizontally heterogeneous erosion parameters.

Erosion depths in the microcosm and Delta are on the order of a floc diameter. For a typical $m_{0.4}$ of 0.05 kg/m^2 and bed density of 600 kg/m^3, the erosion depth would be about 80 μm which is the same order of magnitude as the diameter of a single suspended floc (Ganju et al. 2007; Manning and

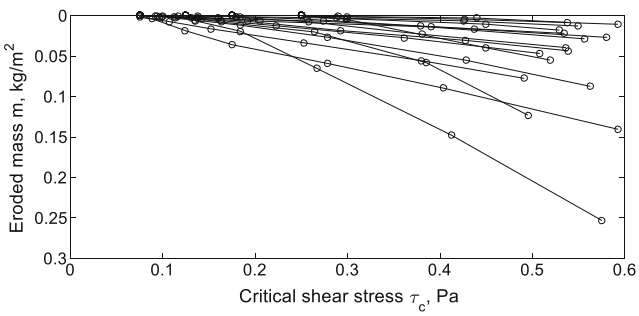

Fig. 4 Critical shear stress measurements for 15 cores from Franks Tract. The *vertical axis* of eroded mass increases down the page to mimic depth dependency

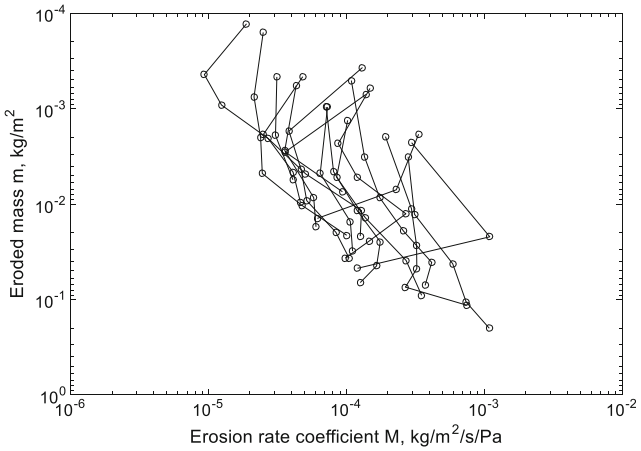

Fig. 5 Erosion rate coefficient computed from erosion microcosm data for 15 cores from Franks Tract. The *vertical axis* of eroded mass increases down the page to mimic depth dependency

Schoellhamer 2013). An eroded mass of 0.05 kg/m^2 would increase SSC 10 mg/l when water depth is 5 m or 50 mg/l when water depth is 1 m. These are typical tidal variations of SSC observed in the Delta. These small erosion depths indicate that sediment is supply limited in the Delta as found by Hestir et al. (2013). Achete et al. (2015) developed a numerical model of sediment transport in the Delta and found that model spin-up was best achieved with an initial condition of no erodible sediment, which is consistent with a supply-limited condition.

The results of the erosion experiments are not consistent with a depth-dependent and horizontally homogeneous erosion model. No erosion is observed for $\tau < \tau_c$. When τ first exceeds τ_c, the mass of eroded sediment is a small fraction of the total mass eroded during the experiment (Fig. 3) and if its distribution were horizontally uniform, the erosion depth would be only a few microns, less than the floc diameter. Cohesive sediment beds, however, can store mass and erode in units of flocs, as opposed to primary particles (Krone 1974; Pouv et al. 2014; Sharif and Atkinson 2012; Winterwerp et al. 2012). Thus, the observed eroded mass when τ initially exceeds τ_c is much less than the mass that would be eroded if only one layer of uniformly distributed flocs was suspended.

Another discrepancy is between the calculated vertical variation of erosion coefficient M and the cohesive sediment theory. In theory, consolidation and compaction make deeper sediment less erodible and M should decrease with depth (Grabowski et al. 2011). For 27 of 34 cores tested, however, M increases with eroded mass (Fig. 5). Consider a simple cohesive bed for which f is the fraction of the area that can be eroded ($\tau > \tau_c$) with an erosion rate coefficient M_a. The erosion rate for this horizontally heterogeneous model is $E_a = f M_a (\tau - \tau_c)$. If a depth-dependent model was applied to this case, $E_d = M_d(\tau - \tau_c)$. Thus, $M_d = f M_a$. As applied shear stress τ increases, f would increase. As mass is eroded, if the rate of increase of f is greater than the depth-dependent

Table 3 Statistical properties of erosion parameters at Franks Tract and upper Cache Slough

	Franks Tract				Upper Cache Slough			
	n	Mean	Median	SD	*n*	Mean	Median	SD
Fines (percent)	14	43	39	16	10	93	93	4.9
Water content (percent)	10	50	45	12	10	70	71	4.9
Initial τ_c (Pa)	15	0.14	0.125	0.076	10	0.11	0.075	0.059
$m_{0.4}$ (kg/m^2)	15	0.038	0.028	0.038	10	0.14	0.13	0.099

n number of cores analyzed, SD standard deviation

decrease of M_a, $M_d = f M_a$ would increase as applied shear stress and eroded mass increases, as is observed in Fig. 5. Thus, the discrepancy between the theoretical and the observed variation of M could be due to horizontal heterogeneity.

5 Numerical experiment of erosion of horizontal heterogeneity and homogeneous beds

We test the hypothesis that small-depth erosion is controlled by horizontal heterogeneity in addition to depth dependence by developing a simple numerical model that considers horizontal heterogeneity, use it to develop an artificial time series of SSC in an erosion microcosm, then analyze that time series assuming horizontal homogeneity. This informs us how the horizontally homogeneous model interprets horizontally heterogeneous erosion.

5.1 Simulation of microcosm erosion

Initial critical shear stress $\tau_c(0)$ was assumed to be normally distributed. The mean critical shear stress was set equal to the mean value for the erosion microcosm experiments, 0.2325 Pa. The bed was discretized into 30 subareas of $\tau_c(0)$ equally spaced from 0.1 to 3.0 times the mean value. The shear vane test revealed that the standard deviation of the shear strength σ was about 30% of the mean. In addition, σ equal to 1% was simulated to represent a horizontally homogeneous bed. Each subarea represents a different fraction of the bed area as determined by the normal distribution (Fig. 9). The resulting distribution is symmetric about the mean and was extended to almost 0.7 Pa which is greater than the maximum applied shear stress of 0.6 Pa during testing.

Based on data from Franks Tract (Fig. 4), critical shear stress is assumed to increase linearly as mass erodes. To account for horizontally different initial conditions of the bed, assume that there is a hypothetical point at which critical shear stress and eroded mass are both zero (Fig. 10).

Critical shear stress as a function of mass eroded is

$$\tau_c = \frac{m + m_0}{\mathrm{dm}/d\tau_c} \tag{5}$$

in which m is the mass eroded during the experiment, m_0 is the initial eroded mass such that the initial critical shear stress for the experiment can be greater than zero, and $\mathrm{dm}/\mathrm{d}\tau_c$ is the slope of the line relating m and τ_c (Fig. 10). Initial eroded mass m_0 as a function of $\tau_c(0)$ is found be setting $\tau_c = \tau_c(0)$ and $m = 0$ and solving Eq. 5 for

$$m_0 = \tau_c(0)\,\frac{dm}{d\tau_c} \tag{6}$$

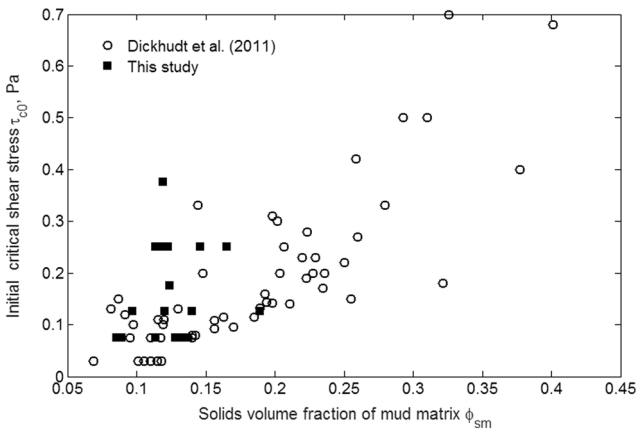

Fig. 6 Initial critical shear stress $\tau_c(0)$ as a function of the solid volume fraction of mud matrix φ_{sm} for data presented by Dickhudt et al. (2011) and the 34 cores analyzed in this study

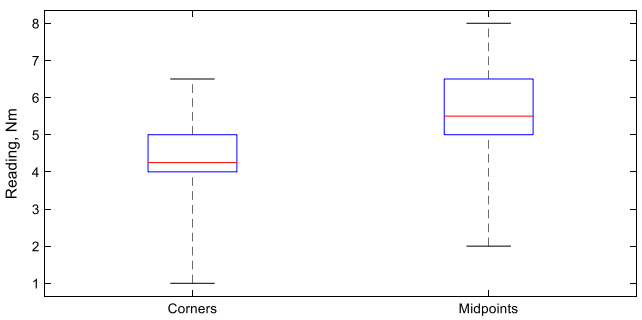

Fig. 7 Boxplots of corner and midpoint results from shear vane readings. The *center horizontal line* is the median, the *upper and lower edges of the boxes* are the upper and lower quartiles, and the *dashed whiskers* indicate the range of data

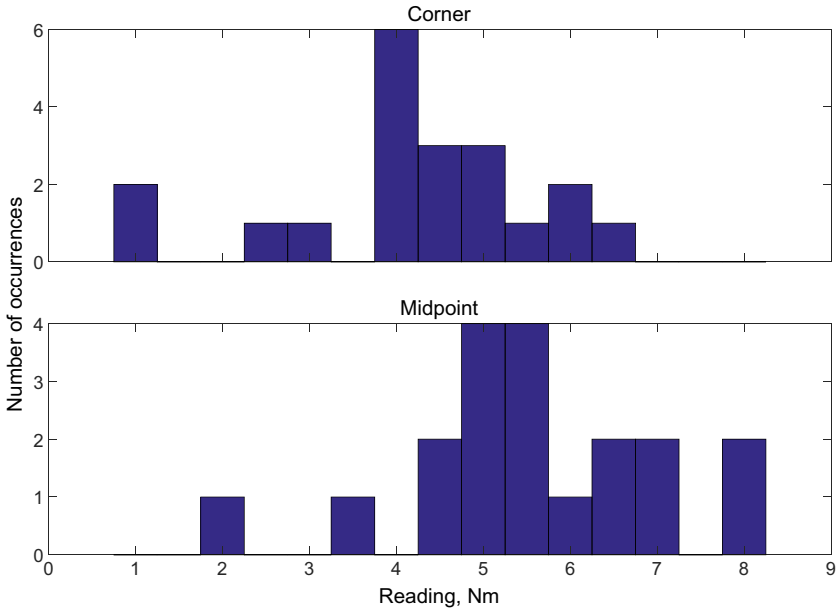

Fig. 8 Histograms of corner and midpoint shear vane readings

From the data on Fig. 5, erosion rate coefficient M is assumed to decrease exponentially with eroded mass

$$M = M_0 e^{-(m+m_0)/m_e} \tag{7}$$

in which M_0 is the hypothetical erosion rate coefficient when $\tau_c = 0$ and m_e is a decay rate. Combine Eqs. 5 and 7 to get M as a function of τ_c

$$M = M_0 e^{-\tau_c/\tau_e} \tag{8}$$

in which

$$\tau_e = \frac{m_e}{\mathrm{d}m/\mathrm{d}\tau_c} \tag{9}$$

The model initially calculates the initial eroded mass m_0 for each subarea with Eq. 6. At each time and for each subarea, the critical shear stress is calculated with Eq. 5. At time t for subarea a, erosion rate $E(t,a)$ and mass eroded during the experiment $m(t,a)$ are

$$E(t,a) = M_0 e^{-\frac{\tau_c(t,a)}{\tau_e}}(\tau(t) - \tau_c(t,a)) \tag{10}$$

$$m(t,a) = m(t-\Delta t, a) + E(t,a)\Delta t \tag{11}$$

for excess shear stress $\tau(t) - \tau_c(t,a) > 0$; otherwise, $E(t,a) = 0$. The model time step is Δt. SSC in the erosion chamber

$$C(t) = C(t-\Delta t)\left(1 - \frac{Q(t)\Delta t}{V}\right) + \sum_a f(a)E(t,a)\Delta t A/V \tag{12}$$

in which $Q(t)$ is the flow rate through the erosion microcosm, V is the volume of the erosion microcosm (7.854×10^{-4} m^3), $f(a)$ is the fraction of the total area

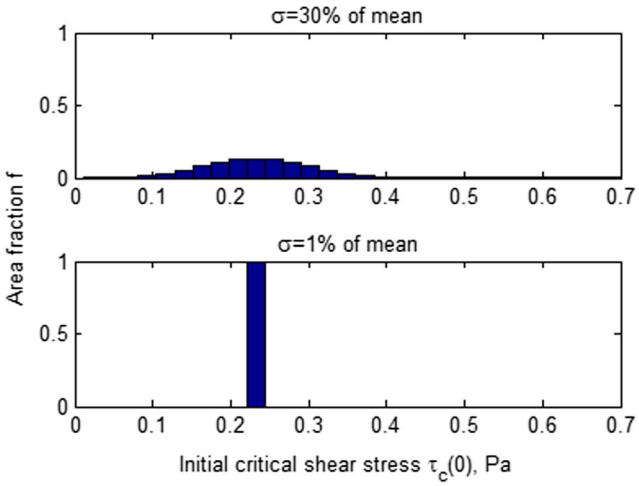

Fig. 9 Distribution of initial critical shear stress $\tau_c(0)$ for σ equal to 30 and 1% of the mean $\tau_c(0)$ (0.2325 Pa)

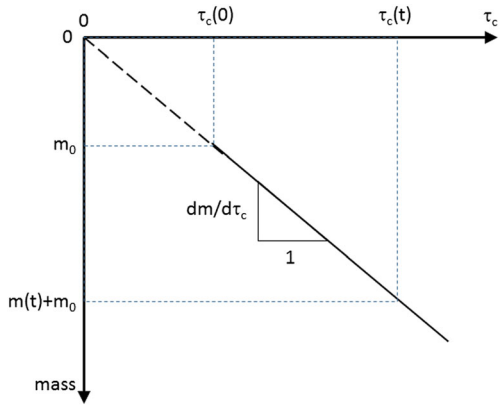

Fig. 10 Eroded mass and critical shear stress τ_c are assumed to be linearly related with a slope of $\mathrm{d}m/\mathrm{d}\tau_c$. Initial critical shear stress $\tau_c(0)$ corresponds to an initial eroded mass m_0 such that if $\tau_c(0)$ was zero, the eroded mass would be zero. At time t, the mass eroded during the experiment is $m(t)$ and the critical shear stress is $\tau_c(t)$

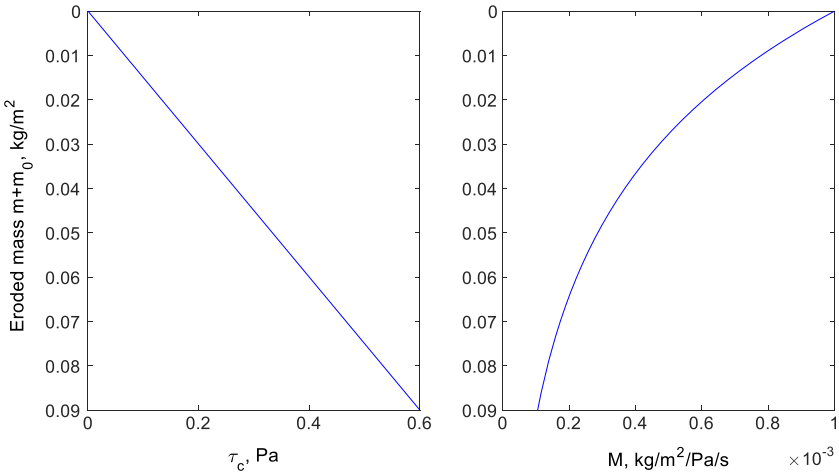

Fig. 11 Variation of critical shear stress τ_c and erosion rate coefficient M with eroded mass $m + m_0$

represented by subarea a (Fig. 9), and A is the total sediment surface area (0.0076 m^2). SSC of inflowing water is assumed to equal zero, and deposition is assumed to be negligible.

Model coefficients were selected to be representative of data from Franks Tract. Linear regression of data on Fig. 4 produces a slope $dm/d\tau_c = 0.15$ kg/m^2/Pa ($n = 112$, $r^2 = 0.40$, $p < 0.001$). Erosion rate coefficient M varies from 10^{-4}–10^{-3} kg/m^2/s/Pa (Fig. 5). For this model, we assume that $M_0 = 0.001$ kg/m^2/s/Pa. A value of $m_e = 0.04$ kg/m^2 was selected, because it gives about an order of magnitude decrease in M for typical final experimental values of $m + m_0$. The resulting τ_c and M as functions of $m + m_0$ used in the model are shown in Fig. 11. A 1-s time step Δt was used, the initial SSC was zero, and the applied shear stresses used in an actual experiment and flow rates for a water temperature of 15 °C (Table 1) were applied in ascending order every 1200 s.

Simulated SSC for the heterogeneous bed ($\sigma = 30\%$ of the mean, Fig. 12) is similar to experimental SSC (Fig. 3). Simulated erosion begins when the applied shear exceeds the smallest initial critical shear stress (0.02325 Pa, one tenth of the mean). Only 0.15% of the bed area was eroding, so SSC is three orders of magnitude less than its value at the end of the simulated experiment. Erosion is supply limited (type I erosion, Sanford and Maa (2001)) as there is an initial increase in SSC for each step followed by a decrease. Overall, erosion and SSC gradually increase throughout the experiment.

The gradual increase in SSC makes identification of a singular critical shear stress difficult and subjective, as is found when interpreting observed microcosm data (Fig. 3). If SSC measurement noise and variation of the inflowing SSC were about 10^{-3} kg/m^3, the first two or three erosion events in Fig. 12 would likely be obscured and the critical shear stress would be poorly defined.

For the final three shear steps, SSC for the homogeneous bed is slightly greater than for the heterogeneous bed because all of the homogeneous bed is eroding while not all of the heterogeneous bed is eroding. For the horizontally homogeneous bed ($\sigma = 1\%$ of the mean), erosion starts and SSC suddenly increases when shear is increased from 0.2 to 0.3 Pa, clearly indicating that the critical shear stress

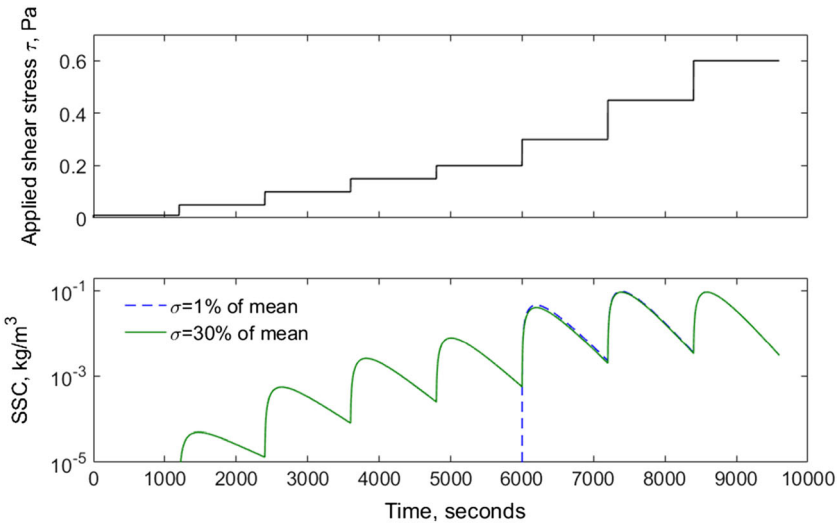

Fig. 12 Applied shear stress and resulting suspended-sediment concentration (SSC) for the numerical model. *Solid line in the lower plot* represents heterogeneous bed; *dashed line* is homogeneous bed

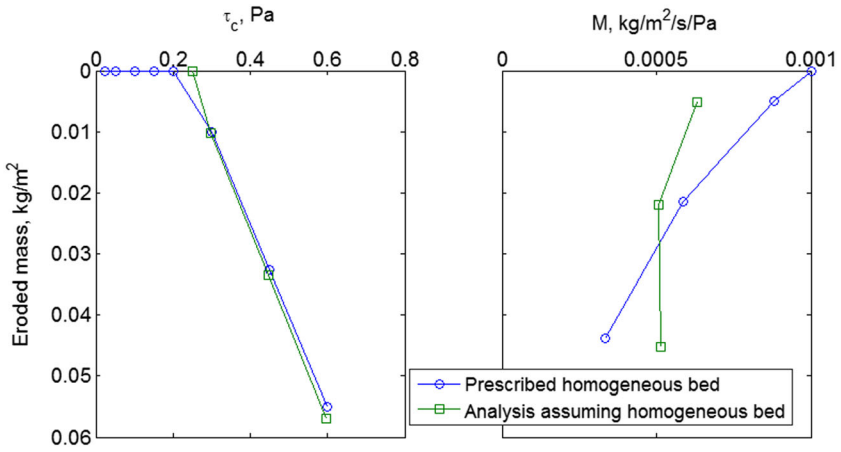

Fig. 13 Critical shear stress τ_c and erosion rate coefficient M as functions of eroded mass for a prescribed horizontally homogeneous bed and from analysis of artificial microcosm data assuming a horizontally homogeneous bed. The prescribed horizontally homogeneous bed has an initial mean critical shear stress of 0.2325 Pa and a normal distribution for which the standard deviation is 1% of the mean (Fig. 9). This bed is equivalent to a horizontally homogeneous bed for which a depth-dependent erosion model is applicable. Erosion rate coefficient M for the prescribed bed is calculated with Eq. 8 for which eroded mass equals $m + m_0$

(0.2325 Pa) is between these two values. This clear indication of the onset of erosion is absent from the simulated heterogeneous bed SSC and from measured data (Fig. 3).

5.2 Analysis of artificial erosion data assuming the bed is homogeneous

The artificial SSC time series in the previous section (Fig. 12) were developed by assuming two different scenarios: horizontally homogeneous and heterogeneous erosion. In this section, we apply the analysis software for the microcosm to these time series. This demonstrates how horizontally heterogeneous erosion would be interpreted by assuming horizontal homogeneity. The results are compared to observed microcosm data to test the hypothesis that shallow depth erosion is horizontally heterogeneous.

The prescribed relation between eroded mass and critical shear stress is reproduced when artificial microcosm data are analyzed assuming that the bed is horizontally homogeneous whether the bed is nearly homogeneous (σ = 1% of the mean, Fig. 13) or heterogeneous (σ = 30% of the mean, Fig. 14). Thus, mass-limited erosion of a horizontally heterogeneous bed (Fig. 14) is correctly represented by a model that assumes horizontal homogeneity.

The prescribed relation between eroded mass and erosion constant M for a horizontally heterogeneous bed is not reproduced by analyzing erosion microcosm data assuming a horizontally homogeneous bed (Fig. 14). The prescribed M decreases with eroded mass while M determined by assuming a horizontally homogeneous bed increases with eroded mass. The calculation of M assumes that the entire bed erodes, so calculated M includes a factor for the fraction of area eroding which increases with eroded mass. If the bed is nearly

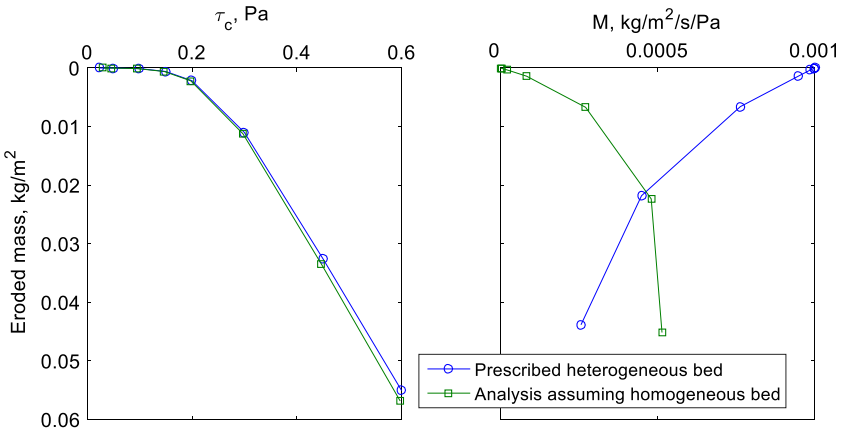

Fig. 14 Critical shear stress τ_c and erosion rate coefficient M as functions of eroded mass for a prescribed horizontally heterogeneous bed and from analysis of artificial microcosm data assuming a horizontally homogeneous bed. The prescribed horizontally heterogeneous bed has an initial mean critical shear stress of 0.2325 Pa and a normal distribution for which the standard deviation is 30% of the mean (Fig. 9). Erosion rate coefficient M for the prescribed bed is calculated with Eq. 8 for which eroded mass equals $m + m_0$

Table 4 Numerical experiment characteristics of homogeneous and heterogeneous cohesive sediment beds

	Homogeneous bed	Heterogeneous bed
Initial critical shear stress $\tau_c(0)$	Well defined, easy to estimate	Poorly defined, difficult to estimate
Erosion rate coefficient M	Decreases as eroded mass increases	If data are analyzed assuming the bed is homogeneous, M increases as eroded mass increases
Suspended-sediment concentration	Sudden increase when τ first exceeds $\tau_c(0)$	Gradual increase with τ

homogeneous (σ = 1%, Fig. 13), M decreases with depth as prescribed.

6 Discussion

The numerical experimental revealed different characteristics of erosion of heterogeneous and homogeneous beds that are summarized in Table 4. Initial critical shear stress, direction of change of the erosion rate coefficient with eroded mass, and the rate of increase of SSC as applied shear stress increases all differ. Small depths of cohesive sediment erode in the Delta, and the characteristics of the empirical data are similar to the simulated heterogeneous bed, not the homogeneous bed. Thus, we conclude that small-depth erosion is controlled by horizontal heterogeneity in addition to depth dependence.

The difficulty in estimating $\tau_c(0)$ from empirical data may account for the poor comparison of some of our data with those presented by Dickhudt et al. (2011) in Fig. 6. Tolhurst et al. (2000) found that intertidal flat cores with relatively high water content and thus low φ_{sm} were more stable (higher $\tau_c(0)$), because stabilizing diatom biofilms were present. This observation also differs from the data presented by Dickhudt et al. (2011). The largest values of $m_{0.4}$ in the Delta (Table 3) were about equal to the smallest values in the York River (Dickhudt et al. 2011), indicating that Delta sediments were less erodible. Whether our high values of $\tau_c(0)$ and low φ_{sm} in Fig. 6 were due to biostabilization or difficulty in identifying a smaller erosion threshold is not known.

Previously, we introduced a simple cohesive bed for which f is the fraction of the area that can be eroded ($\tau > \tau_c$) with an erosion rate coefficient M_a. For this simple bed, the erosion rate $E_a = f M_a (\tau - \tau_c)$ is equivalent to the supply-limited model presented by van Kessel et al. (2011) and van Maren et al. (2015). In their model, erosion rate depends linearly on the amount of sediment below the threshold M_0/M_1 between supply and transport-limited conditions

$$E = mM_1\left(\frac{\tau}{\tau_c}-1\right), m < \frac{M_0}{M_1} \quad (13)$$

$$E = M_0\left(\frac{\tau}{\tau_c}-1\right), m > \frac{M_0}{M_1} \quad (14)$$

For transport-limited conditions, setting f = 1 and equating E_a with Eq. 14 gives $M_0 = M_a\tau_c$. Equating E_a and Eq. 13 for supply-limited conditions gives f = $m/(M_0/M_1)$. Thus, the fraction of area that can be eroded is equivalent to the van Kessel et al. (2011) and van Maren et al. (2015) ratio of bed sediment mass and mass at the threshold between supply- and transport-limited conditions.

The horizontally heterogeneous erosion model starts with a normal distribution of critical shear stress (Fig. 9), but as more compartments begin to erode as τ increases, the distribution becomes nearly uniform with $\tau_c = \tau$. The horizontal heterogeneity of critical shear stress must come from horizontal variation of the erosion rate coefficient $M(m)$, bioturbation/biostabilization, applied shear stress, or deposition. None of these is included in this model which was developed to test our hypothesis, not to be a general model of a cohesive sediment bed. Note that the bed surface can vary in height at the millimeter scale (Fig. 2), and thus, the applied shear stress would not be horizontally uniform.

In practice, it is typically not feasible to simulate (or know) the horizontal heterogeneity of the bed at subcentimeter detail, or the variation in critical shear stress that can exist at any given instant. In this case, a linear equilibrium model is proposed to describe the relationship between instantaneous excess shear stress and erosion rate.

As applied shear stress is increased by an amount $\Delta\tau_c$, the critical shear stress of cohesive sediment beds undergoing small-depth erosion rapidly rises to match the applied shear stress because the increment of eroded mass is small. In this case, rapid means that the time scale for the critical shear stress to increase to the applied stress is small compared to the time over which the mean flow changes significantly and thus small-depth erosion is synonymous with supply-limited erosion. In other words, the bed responds essentially instantaneously to changes in applied bed shear stress. Thus, the variation of critical shear stress with eroded mass (Fig. 10) controls erosion and the erosion rate is unimportant. The mass eroded during a time step would be $dm/d\tau_c \times \Delta\tau_c$. The empirically determined erosion coefficient, which otherwise introduces some uncertainty in the model (Eq. 1), is not used.

In the case of a large mass of bed sediment with uniform critical shear stress less than applied shear stress,

erosion is transport limited, the bed would not respond rapidly to changes in applied shear stress, and erosion rate would be a function of the erosion coefficient. Such a case would occur if erosive properties were uniform with depth, and the small-depth erosion hypothesis would not apply.

Our erosion model is similar to that of Maa and Kim (2002) who analyzed in situ flume and tripod data from the York River and concluded that erosion occurred only during accelerating flows and was close to equilibrium. They assumed a homogeneous bed and that M and excess shear stress $\tau - \tau_c$ were constants, and thus, erosion rate E was a constant when flow was accelerating and zero otherwise. Our erosion model replaces these assumptions with empirical data on $dm/d\tau_c$ and the assumption that the bed is in dynamic equilibrium with the time-varying applied shear stress.

7 Conclusions

Erosion microcosm data from the Sacramento-San Joaquin River Delta and a numerical experiment indicate that small-depth erosion is controlled by horizontal heterogeneity in addition to depth dependence. Specific conclusions are

- If erosion of cohesive sediment in the Delta were horizontally uniform, erosion depths would be about one floc diameter.
- The horizontal standard deviation of critical shear stress in the Delta at Franks Tract is about 30% of the mean value.
- A homogeneous bed has a well-defined initial critical shear stress that is easy to estimate from erosion microcosm data. A heterogeneous bed has a poorly defined initial critical shear stress that is difficult to estimate from erosion microcosm data.
- Analysis of erosion microcosm data with the assumption that the bed is horizontally homogeneous can result in erosion rate coefficients that increase rather than decrease with eroded mass.
- For small-depth erosion, equilibrium between applied and critical shear stress is reached rapidly, so the quantity $dm/d\tau_c$ obtained from erosion microcosm data provides a simple empirical erosion model for accelerating flows. The empirically derived erosion coefficient $M(m)$ is not needed in this approach.

Acknowledgements We thank Kurt Weidich for collecting most of the erosion microcosm data, Pat Dickhudt for providing analysis software, Jan Thompson for explanations of benthic critters, Fernanda Achete and two anonymous reviewers for their constructive comments on this article, and the California Department of Water Resources and the US Bureau of Reclamation for supporting this study. Professor Manning's contribution to this study was partly funded by both US Geological Survey Co-operative Agreement Awards (G11AC20352 and G16AC00314) with HR Wallingford (DDS0280 and DDS1252), and HR Wallingford Company Research project 'FineScale - Dynamics of Fine-grained Cohesive Sediments at Varying Spatial and Temporal Scales' (DDY0523).

References

Achete FM, van der Wegen M, Roelvink D, Jaffe B (2015) A 2-D process-based model for suspended sediment dynamics: a first step towards ecological modeling. Hydrol Earth Syst Sci 19:2837–2857

Andersen TJ, Lanuru M, van Bernem C, Perjup M, Reithmuller R (2010) Erodibility of mixed mudflat dominated by microphytobenthos and *Creastoderma edule*, East Frisian Wadden Sea, Germany. Estuar Coast Shelf Sci 87:197–206

Bentley SJ, Swales A, Pyenson B, Dawe J (2014) Sedimentation, bioturbation, and sedimentary fabric evolution on a modern mesotidal mudflat: a multi-tracer study of processes, rates, and scales. Estuar Coast Shelf Sci 141:58–68

Dickhudt PJ, Friedrichs CT, Sanford LP (2011) Mud matrix solids fraction and bed erodibility in the York River estuary, USA, and other muddy environments. Cont Shelf Res 31:S3–S13

Ganju NK, Schoellhamer DH, Murrell MC, Gartner JW, Wright SA (2007) Constancy of the relation between floc size and density in San Francisco Bay. In: Maa JPY, Sanford LP, Schoellhamer DH (eds) Estuarine and coastal fine sediments dynamics. Elsevier, pp 75–91

Grabowski RC, Droppo IG, Wharton G (2011) Erodibility of cohesive sediment. The importance of sediment properties: Earth-Science Reviews 105:101–120

Gust, G., Mueller, V. (1997). Interfacial hydrodynamics and entrainment functions of currently used erosion devices. In: Burt, N., Parker, R., Watts, J. (eds.), Cohesive sediments. Wallingford, UK. pp. 149–174.

Hayter EJ (1986) Estuarial sediment bed model. In Mehta AJ (ed.), Lecture notes on coastal and estuarine studies, estuarine cohesive sediment dynamics: Springer-Verlag, New York, 14:326–359.

Helsel DR, Hirsch RM (1992) Statistical Methods in Water Resources. Studies in Environmental Science 49:76

Hestir EL, Schoellhamer DH, Morgan TL, Ustin SL (2013) A step decrease in sediment concentration in a highly modified tidal river delta following the 1983 El Niño floods. Mar Geol 345:304–313

Jones NL, Thompson JK, Monismith SG., 2008, A note on the effect of wind waves on vertical mixing in Franks Tract, Sacramento-San Joaquin Delta, California: San Francisco Estuary and Watershed Science 6(2) http://escholarship.org/uc/item/7sk8z936

Krone RB (1974) Engineering interest in the benthic boundary layer. In: McCave IN (ed) The benthic boundary layer. Penum Press, New York, pp 143–156

Maa JPY, Kim SC (2002) A constant erosion rate model for fine sediment in the York River. Virginia: Environmental fluid Mechanics 1:345–360

Manning AJ, Schoellhamer DH (2013) Factors controlling floc settling velocity along a longitudinal estuarine transect. Mar Geol 345:266–280

Morgan-King TL, Schoellhamer DH (2013) Suspended-sediment flux and retention in a backwater tidal slough complex near the landward

boundary of an estuary. Estuar Coasts 36(2):300–318 http://link.springer.com/article/10.1007/s12237-012-954-z

Nobriga ML, Feyrer F, Baxter RD, Chotkowski M (2005) Fish community ecology in an altered river delta: spatial patterns in species composition, life history strategies, and biomass. Estuaries 28(5):776–785

Pouv KS, Besq A, Guillou SS, Toorman EA (2014) On cohesive sediment erosion: a first experimental study of the local processes using transparent model materials. Adv Water Resour 72:71–83

Sanford LP, Maa JP-Y (2001) A unified erosion formulation for fine sediments. Mar Geol 179:9–23

Sharif AR, Atkinson JF (2012) Model for surface erosion of cohesive soils. J Hydraul Eng 138(7):581–590

Swanson KM, Drexler JZ, Fuller C, Schoellhamer DH (2015) Modeling tidal freshwater marsh sustainability in the Sacramento-San Joaquin Delta under a broad suite of potential future scenarios: San Francisco Estuary and Watershed Science 13(1). http://escholarship.org/uc/item/7x65r0tf.

Tolhurst TJ, Riethmuller R, Paterson DM (2000) In situ versus laboratory analysis of sediment stability from intertidal mudflats. Cont Shelf Res 20:1317–1334

van Prooijen BC, Winterwerp JC (2010) A stochastic formulation for erosion of cohesive sediments. J Geophys Res 115:C01005. doi:10.1029/2008JC005189

van Kessel T, Winterwerp H, van Prooijen B, van Ledden M, Borst W (2011) Modelling the seasonal dynamics of SPM with a simple algorithm for the buffering of fines in a sandy sea bed. Cont Shelf Res 31:S124–S134. doi:10.1016/j.csr.2010.04.008

van Maren DS, van Kessel T, Cronin K, Sittoni L (2015) The impact of channel deepening and dredging on estuarine sediment concentration. Cont Shelf Res 95:1–14

Winterwerp JC, van Kesteren WGM, van Prooijen B, Jacobs W (2012) A conceptual framework for shear flow-induced erosion of soft cohesive sediment beds. J Geophys Res 117:C10020

Wright SA, Morgan TL (2015) Suspended sediment transport through a large fluvial-tidal channel network. Proceedings of the 10th Federal Interagency Sedimentation Conference, Reno, NV, April 19–22, 2015, pp 1522–1533 http://www.sedhyd.org/2015/openconf/modules/request.php?module=oc_proceedings&action=summary.php&a=Accept&id=173